eISSN: 2976-1190

**Journal of Engineering and Sciences**

Vol. 3 Issue 2 Nov 30, 2024

*DOI: https://doi.org/10.3126/jes2.v3i2.72184*

*Journal homepage: **Journal of Engineering and Sciences (nepjol.info)***

Publisher: Research Management Cell, Pashchimanchal Campus, Lamachour, Pokhara

# Molecular Simulation of $H_2O$ Adsorption in Mg-MOF-74

Bishwas Adhikari[1], Anup Subedi[1], Aabiskar Bhusal[2,*], Kapil Adhikari[2,3]

[1]*Prithvi Narayan Campus, Pokhara,* Nepal

[2]*Physics Research Initiatives, Pokhara, Nepal*

[3] *Gandaki University, Pokhara, Nepal*

**Corresponding author. Email: aabiskar@pri.org.np*

*(Manuscript Received: 08/09/2024; Revised: 29/09/2024; Accepted: 01/10/2024)*

**Abstract**

Amidst a global challenge of increasing water scarcity, atmospheric water harvesting (AWH) has surfaced as a hopeful solution. Metal-organic frameworks (MOFs) are highly esteemed among porous materials for their wide-ranging use in the field of water adsorption. This study specifically focuses on investigating the water adsorption capacity of Mg-MOF-74. A hybrid GCMC/MD simulation in LAMMPS was employed to study the water uptake with respect to pressure at a constant temperature of 298 K, the adsorption site of water in the framework, and the interaction energy between them. The end results suggest that Mg-MOF-74 exhibits promising potential as an effective adsorbent for atmospheric water harvesting, boasting a decent uptake of 25.172 $mmol/g$ even at a low pressure of 1 bar. Furthermore, radial distribution function (RDF) analysis reflects the importance of the open metal site in the framework, closer to which the adsorbed water molecules can be seen. Water uptake increases as the pressure increases, which decreases the diffusion coefficient. At the same time, the interaction energy between water and the framework becomes more and more negative with an increase in pressure.

***Keywords:*** Metal-Organic Frameworks; Water adsorption; Molecular Dynamics; Diffusion coefficient; Pressure

## 1. Introduction

Water resource is the most important part of biotic life because nothing in the world can replace fresh water and its pivotal role in the existence of living organisms on the earth (Shiklomanov, 1998). Water is found in our planet in all three states; almost 71% of the earth is covered with water part, but about 97.5% of it is salty water, and only 2.5% is freshwater, of which just 0.26% is present on the surface of the earth in liquid form (Mishra, 2023). However, despite this fact, the problem of water scarcity is increasing daily (Mekonnen & Hoekstra, 2016). Although people from coastal regions use seawater after various purification techniques like filtration, distillation, and so on, inland communities cannot do so. In this case, researchers have turned their focus towards atmospheric water. This process of harvesting water present in the atmosphere is termed atmospheric water harvesting (AWH) (Lee, et al., 2012).

Water is retained in the Earth's atmosphere either as water droplets or vapor, constituting approximately 10% of freshwater sources and contributing to a total volume of around 50,000 $km^3$ (Zhou et al., 2020). To harvest water from this rich ore, various porous materials, including zeolites, activated carbon, activated alumina, silica gel, as well as organic materials and metal-organic composites, have been extensively studied as adsorbents (Li et al., 2009). But recently, metal-organic frameworks (MOFs) have drawn considerable attention (Pan et al., 2020;

Xu & Hu, 2023).
MOFs are crafted by linking metal ions with organic ligands or connectors, and their appeal has grown significantly in recent times (Yuan et al., 2018; Zafar & Sharmin, 2016). Compounds of this kind exhibit an extensive surface area (Chae et al., 2004), coupled with the ability to modify pore sizes and a diverse, aesthetically pleasing structure (Soni et al., 2020). Because of these properties, MOFs have been sparking considerable interest across various fields, including clean energy (Emam et al., 2020), biomedical imaging (Della et al., 2011), sensing (Kreno et al., 2012), drug delivery (Wu & Yang, 2017), destroying toxic chemicals (Moghadam et al., 2016), purifying water (Hasan & Jhung, 2015), storing and separating gases (Li & Yang, 2007), magnetic resonance imaging (MRI) (Chowdhury, 2017), among others.

From a pool of thousands of MOFs, selecting an appropriate one suitable for water harvesting is difficult. The search for optimal water harvesters is about achieving a balance between high sorption capacity, energy efficiency, speed and durable performance, all of which contribute to the effectiveness and sustainability of atmospheric water harvesting systems (Zhou et al., 2020). In the initial time of MOF synthesizing, researchers encountered the problem of low stability of MOF in the presence of water. However, this problem has been solved today, and many MOFs with high water stability have been synthesized (Kalmutzki et al., 2018). MOF harvesters have become the first material in the history of science and technology to produce drinking water from desert air (Xu & Yaghi, 2020). MOFs are versatile in water applications, serving not only for adsorption but also for purification by removing organic contaminants, such as herbicides, pesticides, and heavy metals (Petit, 2018).
Among the wide varieties of MOFs which has been synthesized and studied, M-MOF-74 (where M represents the metal like Zn, Mg, Co, Ni, etc.) is one of the families of MOF with promising features adequate to attract lots of attention (Zuluaga et al., 2016; Degaga, 2018). Extensively investigated through both computational simulations and experimental synthesis, these isostructural microporous MOFs feature uniform hexagonal pores (Howe et al., 2017). The 2,5-dioxido-1,4-benzene-dicarboxylate (dobdc) linkers that make up this MOF have huge one-dimensional pores with a diameter of around 12Å, which are connected by helical chains of $M^{2+}$ at their intersections (Adhikari et al., 2024; Pham et al., 2015).
The harmonious interaction between the metal ions and organic linkers in M-MOF-74 creates a distinctive environment for water molecules, resulting in impressive adsorption capacities and rapid adsorption-desorption kinetics (Kalmutzki et al., 2018; Schoenecker at al., 2012). Mg-MOF-74 has the capacity to uptake up to 0.54 g/g of water below 10% relative humidity while maintaining its structure (Li et al., 2015). At 298K, Mg-MOF-74 has shown high water as well as carbon-dioxide adsorption, i.e., 593 $mL/g$ and 350 $mg/g$ respectively (Yang et al., 2012).
In this work, Mg-MOF-74 was thoroughly studied to understand its water adsorption capacity. Using hybrid GCMC/MD simulation, water was adsorbed into the MOF framework, and its adsorption and diffusion characteristics were studied. GCMC was used because of its unique capability of directly determining the number of moles of molecules within the pores of any material (Yun et al., 2002). Molecular dynamics was selected over methods like Hartree Fock (Slater, 1951) and Density Functional Theory (DFT) (Engel, 2011) because once an appropriate potential is selected, MD is cheaper, faster, and can be considered one of the most efficient methods to look into the interaction of atoms and molecules at the molecular level (Hospital et al., 2015; Mao et al., 2023). Furthermore, the adsorption site of water molecules and the interaction energy between the adsorbate and the adsorbent were also studied.

## 2. Models and Methods

*2.1 Simulation details*

In this work, simulations of $H_2O$ adsorption was performed in a triclinic Mg-MOF-74 structure, which was taken from Adhikari et al. (2024). The primitive unit cell structure considered consisted of 54 atoms, including 6 magnesium centers, and its lattice parameters were a = 6.72281 Å, b = 15.3622 Å, and c = 15.3261 Å.

After an optimized structure of Mg-MOF-74 was taken from the above-mentioned literature, Gaussian09 (Frisch, 2009) was employed to compute the partial charge of the atoms. B3LYP hybrid functional and the 6-311g(2d,2p) basis set were applied for this. Then, after replicating the MOF into a 4×4×4 supercell structure, the GCMC simulation in Large Scale Atomic/Molecular Massively Parallel Simulator (LAMMPS) code (Plimpton et al., 2007) was performed to simulate the adsorption of water molecules into the replicated MOF.

Universal Force field (UFF) was used for force field parameters of Mg-MOF-74 atoms (Zhang et al., 2023) and the SPC/E model was used to describe the water molecules (Berendsen et al., 1987). Equation (1) is the 12-6 Lennard-Jones and electrostatic interaction potential equation (Mercado et al., 2016), which was used to describe the system. For the unlike atoms of the system, required parameters were calculated using the Lorentz-Berthelot mixing rule, which is represented by equations (2) and (3) (Du et al., 2020). Table 1 lists the LJ parameters and the charges of the atoms used in this work.

$$U_{ij} = 4\varepsilon_{ij}\left[\left(\frac{\sigma_{ij}}{r_{ij}}\right)^{12} - \left(\frac{\sigma_{ij}}{r_{ij}}\right)^{6}\right] + \frac{q_i q_j}{4\pi\varepsilon_o r_{ij}} \quad (1)$$

$$\sigma_{ij} = \frac{\sigma_{ii} + \sigma_{jj}}{2} \quad (2)$$

$$\varepsilon_{ij} = \sqrt{\varepsilon_{ii}\varepsilon_{jj}} \quad (3)$$

Table 1: LJ parameters of atoms used in this work (*Zhang et al., 2023*; *Berendsen et al., 1987;* Chatterjee et al., 2008)

| Atoms | $\varepsilon/k_B$ (K) | $\sigma$ (Å) | $q$ (e) |
|---|---|---|---|
| Mg | 55.8574 | 3.0210 | 1.1151 |
| H | 7.6489 | 3.1950 | 0.1267 |
| C1 | 73.8224 | 3.9830 | -0.1681 |
| C2 | 73.8224 | 3.9830 | 0.1873 |
| C3 | 73.8224 | 3.9830 | -0.0987 |
| C4 | 73.8224 | 3.9830 | 0.6469 |
| O1 | 47.8562 | 3.8983 | -0.6521 |
| O2 | 47.8562 | 3.8983 | -0.5320 |
| O3 | 47.8562 | 3.8983 | -0.6251 |
| H($H_2O$) | 0.000 | 0.000 | 0.4238 |
| O($H_2O$) | 78.1752 | 3.166 | -0.8476 |

During the GCMC simulation in LAMMPS, the Metropolis algorithm (Metropolis et al., 1953) was employed to attempt insertions and deletions of water molecules into our MOF, allowing the system to equilibrate and sample the configuration space (Babaei et al., 2023). To describe the pressure of the system, the fugacity coefficient was calculated using the Peng-Robinson equation of state (PR-EOS) (Peng & Robinson, 1976). A single cycle of GCMC comprising 30 GCMC exchanges was performed every 100-time steps of the simulation, where the MOF structure was kept rigid, and an NVT ensemble was used to ensure that the temperature of the system was stable at 298 K so that the equilibrium state was acquired faster. The NVT ensemble adopted a Nosé-Hover thermostat (Nosé, 1984) with a temperature-damping parameter of 100 fs to control the temperature. In contrast, the time integration step for the whole simulation was set to 1 fs. A cut-off radius of 14 Å was used for the force field, and a particle-particle particle-mesh (PM) solver with a precision of 10 to the precision of $10^{-4}$ was used to compute long-range electrostatic interaction. This simulation consisted of a total of $5\times10^5$steps. To compare the adsorption properties of our MOF structure, the simulation was conducted at different pressures ranging from 1 bar to 10 bar.

After the completion of the GCMC simulation, MD analysis was performed for a total of $1\times10^6$ steps ($5\times10^5$ equilibration steps and the same number of production steps) to elucidate the structural and dynamic characteristics of the system. To study the adsorption site of adsorbed water molecules around the MOF structure, radial distribution function (RDF) analysis (Kirkwood & Boggs, 1942) was done to shed light on the diffusivity of water molecules inside the MOF structure and mean square distribution (MSD) analysis (Listyarini et al., 2023). Additionally, interaction energy analysis (Wang et al., 2021) was also performed to understand the interplay between the adsorbate and the adsorbent molecules.

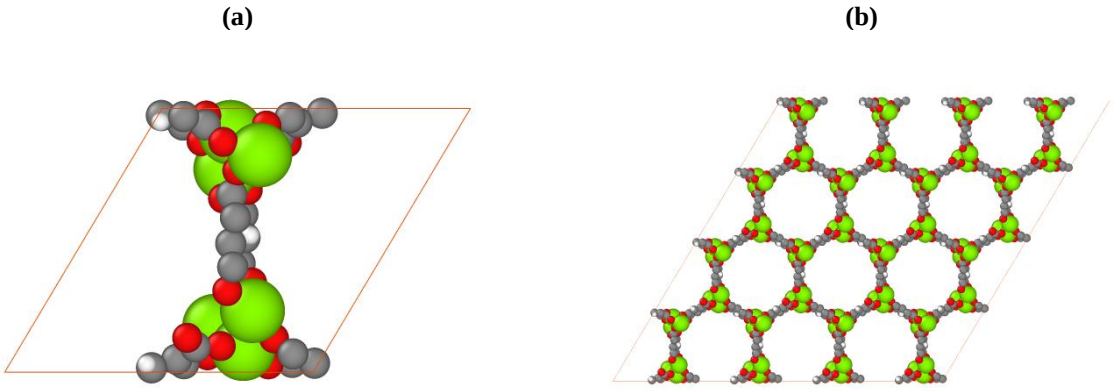


Figure 1: (a) Unit cell structure of Mg-MOF-74 where green = Mg, red = O, grey = C and white = H, (b) 4×4×4 supercell structure of Mg-MOF-74

*2.2 Model validation*

In this section of the study, we validated the proposed model by comparing the phase density of water molecules obtained in this study with data from the National Institute of Standards and Technology (NIST) database (Lemmon, 2010). Phase density of water was calculated through hybrid GCMC/MD simulations. Initially, water molecules were inserted into a 50Å empty cubic box using GCMC simulation, following the procedures outlined in the simulation details section. Subsequently, once equilibrium was achieved, the box's density was computed and compared with

the data obtained from the NIST database. Table 2 compares these datasets, indicating that our calculated density closely aligns with the NIST data, with a relative error of 3.1%. This agreement confirms the validity of using the PR-EOS for calculating the fugacity of water molecules (Shang et al., 2024).

Table 2: Model validation

| Pressure (bar) | Density ($kg/m^3$) | | Relative error (%) |
|---|---|---|---|
| | NIST database | This work | |
| 1 | 997.09 | 982.89 | 1.42 |
| 2 | 997.13 | 990.309 | 0.68 |
| 3 | 997.18 | 980.496 | 1.67 |
| 4 | 997.22 | 983.847 | 1.34 |
| 5 | 997.27 | 982.411 | 1.49 |
| 6 | 997.31 | 980.257 | 1.71 |
| 7 | 997.36 | 978.103 | 1.93 |
| 8 | 997.4 | 977.625 | 1.98 |
| 9 | 997.45 | 980.496 | 1.7 |
| 10 | 997.49 | 967.334 | 3.02 |

## 3. Results and Discussion

### *3.1 Adsorption isotherm*

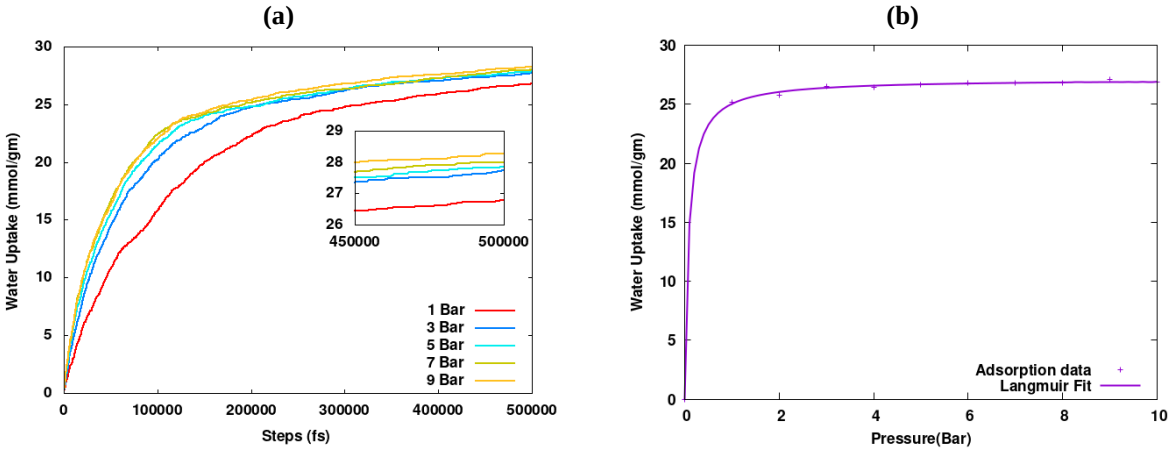


Figure 2: (a) Time evolution of water molecules (mmol/g) in the system, (b) Adsorption isotherm of water for Mg-MOF-74 at 298 K

During the Grand Canonical Monte Carlo (GCMC) simulation, we monitored the accumulation of water molecules within the structure of the MOF over time, as illustrated in Figure 2(a). In each of the plots, the water uptake increases with time, and after around 300,000 steps, the plot starts to saturate and form a plateaued region. This saturation indicates the attainment of the MOF's maximum adsorption capacity, a crucial insight into its performance (Fatriansyah et al., 2019).

To analyze the adsorption behavior comprehensively, we computed the average adsorption of water molecules during the saturated period across different pressure levels and this data was then subjected to fitting using the Langmuir adsorption isotherm model, facilitating the generation of a corresponding graph, as shown in Figure 2(b). The graph depicts a noticeable trend of increasing water uptake with elevated pressure, eventually reaching a saturation point after a few simulation steps in each instance. The graph also reveals distinct uptake values with an uptake of 25.172 $mmol/g$ observed even at low pressure of 1 bar pressure.
Equation (4) represents the approximated form of the Langmuir isotherm equation, which was used to fit the isotherm (Liu, 2006).

$$Q \approx Q_{max} \frac{KC}{1 + KC} \tag{4}$$

where $Q$ is the equilibrium adsorption capacity, $Q_{max}$ is the saturated adsorption capacity, $K$ is the equilibrium constant, and C is the volumetric concentration of the adsorbate.

*3.2 Adsorption sites of water*

RDF is capable of demonstrating the distribution of atoms around any specified atom [55]. So, to study the adsorption site of water around the MOF atoms, RDF is calculated using equation (5)[50].

$$g_{ij}(r) = \frac{N_{ij}(r, r + \Delta r)V}{4\pi r^2 \Delta r N_i N_j} \tag{5}$$

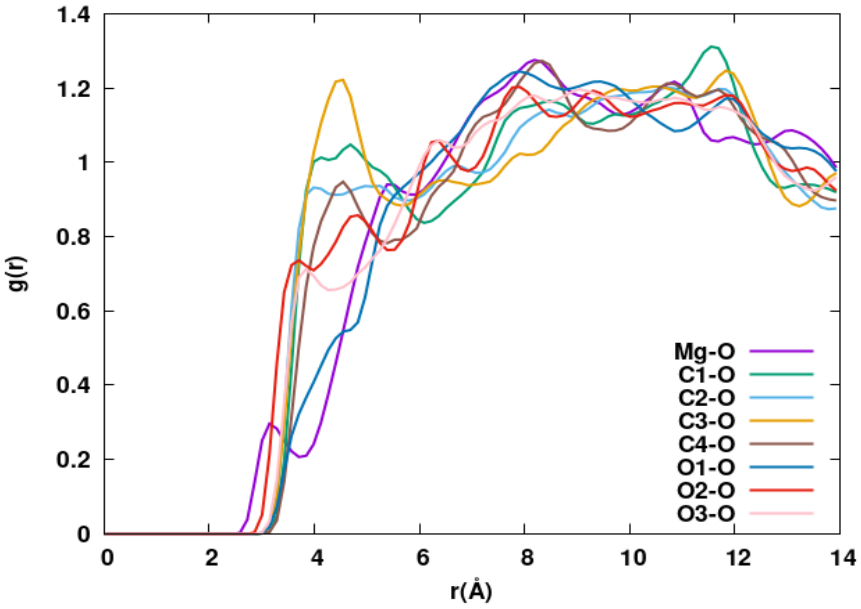


Figure 3: RDFs of water molecules around Mg-MOF-74 framework at 1 bar pressure

where $r$ represents the distance between atoms $i$ and $j$, $N_{ij}(r, r + \Delta r)$ denotes the count of the atom $j$ surrounding atom $i$ within a shell ranging from $r$ to $r + \Delta r$, $V$ represents the volume of the system, and $N_i$ and $N_j$ are the respective counts of atoms $i$ and $j$ in the system.
Figure 3 illustrates the radial distribution functions (RDFs) portraying the adsorption sites of water molecules surrounding the Mg-MOF-74 framework atoms (Mg, $C_1$, $C_2$, $C_3$, $C_4$, $O_1$, $O_2$, and $O_3$) at a pressure of 1 bar. The first characteristic peak in the graph, located at r = 3.16 Å between the Mg

atom of the framework and water molecules, suggests that magnesium atoms serve as the preferred adsorption sites for water molecules. Moreover, the plot also uncovers two distinct peaks signifying the interaction between water molecules and specific atoms within the MOF, specifically $C_3$, and $C_4$, observed at distances of 4.48 Å, and 4.5 Å, respectively. These peaks represent preferred distances for the interaction between $H_2O$ molecules and the specified MOF atoms, suggesting the presence of designated binding sites within the MOF framework that facilitate these interactions. Additionally, the plot indicates that the closest distance between the MOF and water molecules is 2.45Å, signifying repulsion between the atoms of the MOF and water molecules at shorter distances.

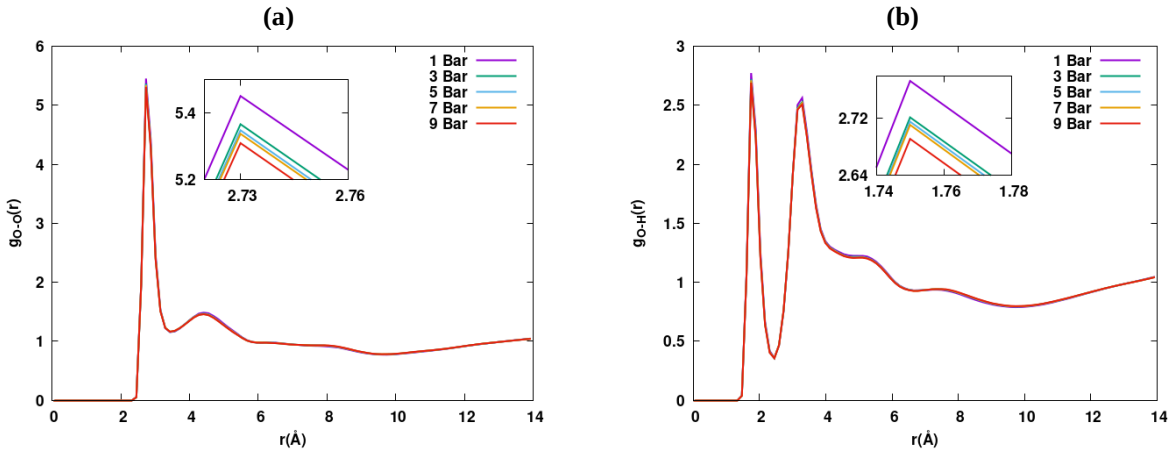


Figure 4 -- RDFs of (a) O-O, (b) O-H of adsorbed water molecules at different pressure

Figure 4(a) depicts the RDFs between oxygen atoms of water molecules within the framework at various pressures. The figure reveals that as pressure increases, the peak of the RDFs decreases, indicating the formation of fewer hydrogen bonds at lower pressures or uptakes compared to higher pressures or uptakes (Wang et al., 2021). Similarly, Figure 4(b) presents the RDFs between H-atoms of different water molecules adsorbed within the MOF structure at varying pressures. The positions of the first peaks in $g_{O-O}(r)$ and $g_{O-H}(r)$ is located at approximately 2.8 Å and 1.8 Å, respectively, which distinctly indicates the presence of stable hydrogen bonds (Demontis et al., 2003). These two graphs also show that the RDF peak decreases with increasing pressure. This phenomenon occurs because at lower loading or pressure, despite the overall fewer number of hydrogen bonds, the ones that are formed are stronger. This results in water molecules being more tightly packed around each other (Fogarty et al., 2014).

To comprehensively examine the stability and behavior of the system, we conducted calculations to determine the interaction energy between water molecules and the MOF-74 framework. This involved analyzing the distribution of interaction energies across different pressure conditions. Figure 5 illustrates the resulting histogram plot, providing insights into the nature of interactions between water and MOF-74 at varying pressures. The negative values observed in the interaction energy histograms signify an attractive force between the adsorbate (water) and the adsorbent (MOF-74) (Wang et al., 2021). Notably, as pressure increases, the interaction energy becomes increasingly negative, indicating larger adsorption tendencies under elevated pressure conditions. The increase in interaction energy observed from 1 bar to 3 bar aligns with the corresponding increase in water uptake depicted in Figure 2(a).

*Interaction energy*

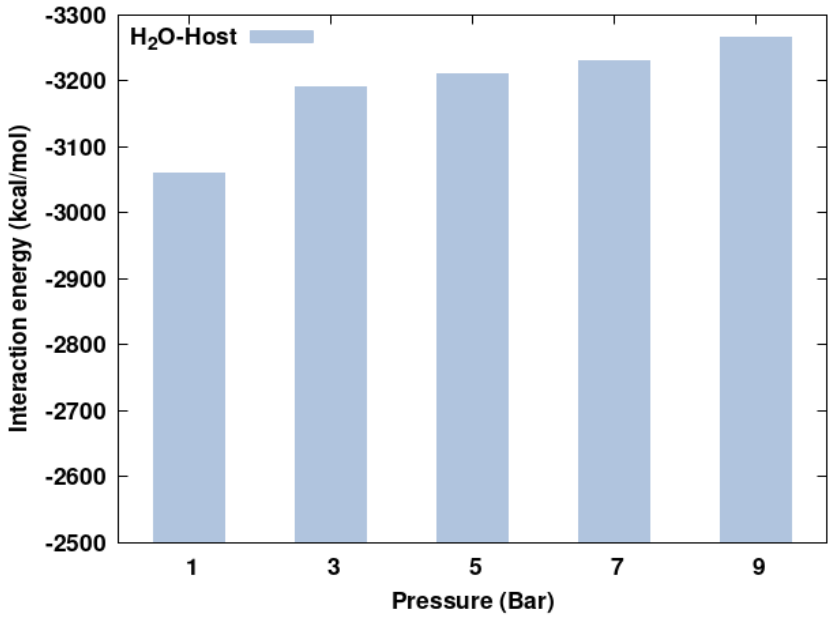


Figure 5: Interaction energy between water molecules and the framework at different pressure

*3.3 Diffusion coefficient of water*

During the MD simulation of this study, Mean Square Displacements (MSDs) for the adsorbed water molecules for each pressure were calculated using equation (6). Thus, the self-diffusion coefficient is calculated using the slope of the MSD-t relationship, which is demonstrated by the equation (7) (Lee, 2016).

$$MSD = \langle \Delta r^2(t) \rangle = \frac{1}{N} \sum_{i=1}^{N} |r_i(t) - r_i(0)|^2 \tag{6}$$

And,

$$D = \frac{1}{6} \frac{d\langle |r(t) - r(0)|^2 \rangle}{dt} = \frac{1}{6} \frac{\langle |r(t) - r(0)|^2 \rangle}{t} \tag{7}$$

The numerical value 6 in the above equation (7) corresponds to the degrees of freedom of atomic jumps in a three-dimensional space, accounting for both forward and backward movements along the considered dimensions.

Figure 6 displays the diffusion coefficient ($D$) of water molecules within the MOF-74 structure under varying pressure conditions. As depicted, there is a noticeable trend of decreasing $D$ with increasing pressure. This phenomenon can be attributed to steric interactions, wherein the average distance between water molecules diminishes as the pressure-induced loading within the MOF structure increases (Salles et al., 2009). This reduction in intermolecular spacing leads to hindered diffusion, resulting in the observed decrease in the diffusion coefficient. This behavior underscores the intricate interplay between pressure, molecular packing, and diffusion dynamics within the MOF environment.

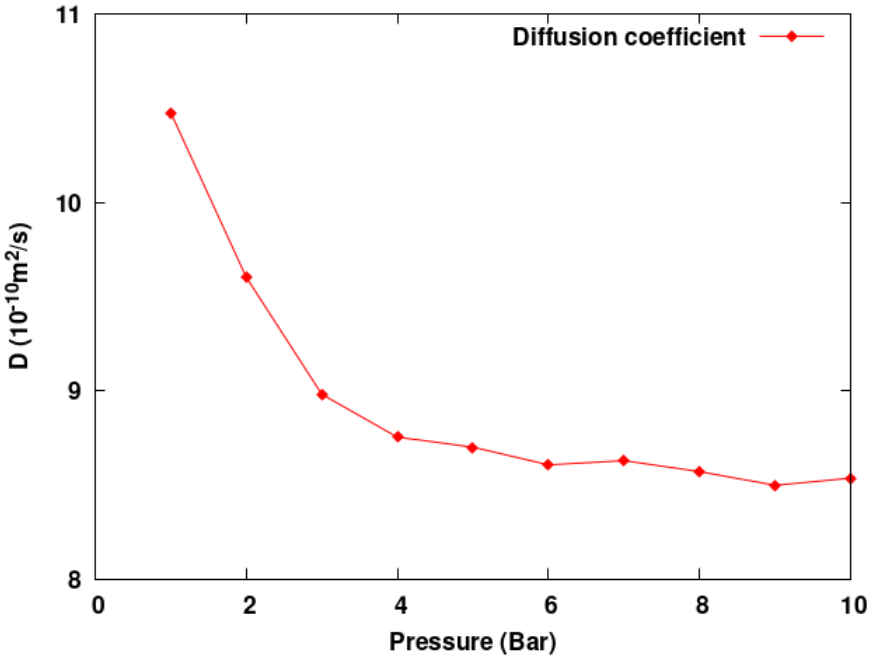


Figure 6: Diffusion coefficient of water at various pressure

## 4. Conclusion

This study is centered on investigating the adsorption behavior of water within the rigid framework of Mg-MOF-74, utilizing a hybrid GCMC/MD simulation approach implemented with LAMMPS. Initially, the average water uptake analysis during the saturation period of the simulation revealed that at 298 K Mg-MOF-74 is capable of harvesting 25.172 $mmol/g$ of water even at a low pressure of 1 bar. Subsequently, we conducted an RDF analysis to elucidate the specific adsorption sites of water molecules, revealing their closer proximity to the metal ion within the framework. Moving forward, we computed the interaction energy between water molecules and the host framework across different pressure conditions to affirm the system's stability. Notably, our results demonstrated that increased pressure leads to a more negative interaction energy, indicating enhanced stability and stronger affinity between water molecules and the framework. Finally, after the analysis of the diffusion coefficient of water along all three spatial directions, our findings indicated an initial decrease in the diffusion coefficient ($D$) with increasing pressure, followed by saturation due to heightened water uptake, thereby reducing the characteristic distance between water molecules.

## References

[1] Shiklomanov, I. A. (1998). *World water resources: A new appraisal and assessment for the 21st century: A summary of the monograph World Water Resources*. UNESCO.

[2] Mishra, R. K. (2023). Freshwater availability and its global challenge. *British Journal of Multidisciplinary and Advanced Studies, 4*(3), 1–78. https://doi.org/10.37745/bjmas.2022.0208

[3] Mekonnen, M. M., & Hoekstra, A. Y. (2016). Four billion people facing severe water scarcity. *Science Advances, 2*(2), e1500323. https://doi.org/10.1126/sciadv.1500323

[4] Lee, A., Moon, M. W., Lim, H., Kim, W. D., & Kim, H. Y. (2012). Water harvest via dewing. *Langmuir, 28*(27), 10183–10191. https://doi.org/10.1021/la3013987

[5] Zhou, X., Lu, H., Zhao, F., & Yu, G. (2020). Atmospheric water harvesting: A review of material and structural designs. *ACS Materials Letters, 2*(7), 671–684. https://doi.org/10.1021/acsmaterialslett.0c00130

[6] Li, J. R., Kuppler, R. J., & Zhou, H. C. (2009). Selective gas adsorption and separation in metal–organic frameworks. *Chemical Society Reviews, 38*(5), 1477–1504. https://doi.org/10.1039/B802426J

[7] Pan, T., Yang, K., & Han, Y. (2020). Recent progress of atmospheric water harvesting using metal-organic frameworks. *Chemical Research in Chinese Universities, 36*, 33–40. https://doi.org/10.1007/s40242-020-9093-6

[8] Xu, H., & Hu, P. (2023). Progress on fundamentals of adsorption transport of metal-organic frameworks materials and sustainable applications for water harvesting and carbon capture. *Journal of Cleaner Production, 393,* 136253. https://doi.org/10.1016/j.jclepro.2023.136253

[9] Yuan, S., Feng, L., Wang, K., et al. (2018). Stable metal–organic frameworks: Design, synthesis, and applications. *Advanced Materials, 30*(37), 1704303. https://doi.org/10.1002/adma.201704303

[10] Zafar, F., & Sharmin, E. (2016). *Metal-organic frameworks*. BoD–Books on Demand. https://doi.org/10.5772/64797

[11] Chae, H. K., Siberio-Pérez, D. Y., Kim, J., et al. (2004). A route to high surface area, porosity and inclusion of large molecules in crystals. *Nature, 427*(6974), 523–527. https://doi.org/10.1038/nature02311

[12] Soni, S., Bajpai, P. K., & Arora, C. (2020). A review on metal-organic frameworks: Synthesis, properties, and application. *Characterization and Application of Nanomaterials, 3*(2), 87–106. https://doi.org/10.24294/can.v3i2.551

[13] Emam, H. E., Abdelhameed, R. M., & Ahmed, H. B. (2020). Adsorptive performance of MOFs and MOF-containing composites for clean energy and a safe environment. *Journal of Environmental Chemical Engineering, 8*(5), 104386. https://doi.org/10.1016/j.jece.2020.104386

[14] Della Rocca, J., Liu, D., & Lin, W. (2011). Nanoscale metal–organic frameworks for biomedical imaging and drug delivery. *Accounts of Chemical Research, 44*(10), 957–968. https://doi.org/10.1021/ar200028a

[15] Kreno, L. E., Leong, K., Farha, O. K., Allendorf, M., Van Duyne, R. P., & Hupp, J. T. (2012). Metal–organic framework materials as chemical sensors. *Chemical Reviews, 112*(2), 1105–1125. https://doi.org/10.1021/cr200324t

[16] Wu, M. X., & Yang, Y. W. (2017). Metal–organic framework (MOF)-based drug/cargo delivery and cancer therapy. *Advanced Materials, 29*(23), 1606134. https://doi.org/10.1002/adma.201606134

[17] Moghadam, P. Z., Fairen-Jimenez, D., & Snurr, R. Q. (2016). Efficient identification of hydrophobic MOFs: Application in the capture of toxic industrial chemicals. *Journal of Materials Chemistry A, 4*(2), 529–536. https://doi.org/10.1039/C5TA06472D

[18] Hasan, Z., & Jhung, S. H. (2015). Removal of hazardous organics from water using metal-organic frameworks (MOFs): Plausible mechanisms for selective adsorptions. *Journal of Hazardous Materials, 283,* 329–339. https://doi.org/10.1016/j.jhazmat.2014.09.046

[19] Li, Y., & Yang, R. T. (2007). Gas adsorption and storage in metal-organic framework MOF-177. *Langmuir, 23*(26), 12937–12944. https://doi.org/10.1021/la702466d

[20] Chowdhury, M. A. (2017). Metal-organic-frameworks for biomedical applications in drug delivery, and as MRI contrast agents. *Journal of Biomedical Materials Research Part A, 105*(4), 1184–1194. https://doi.org/10.1002/jbm.a.35995

[21] Kalmutzki, M. J., Diercks, C. S., & Yaghi, O. M. (2018). Metal–organic frameworks for water harvesting from air. *Advanced Materials, 30*(37), 1704304. https://doi.org/10.1002/adma.201704304

[22] Xu, W., & Yaghi, O. M. (2020). Metal–organic frameworks for water harvesting from air, anywhere, anytime. *ACS Central Science, 6*(8), 1348–1354. https://doi.org/10.1021/acscentsci.0c00678

[23] Petit, C. (2018). Present and future of MOF research in the field of adsorption and molecular separation. *Current Opinion in Chemical Engineering, 20,* 132–142. https://doi.org/10.1016/j.coche.2018.04.004

[24] Zuluaga, S., Fuentes-Fernandez, E. M., Tan, K., et al. (2016). Understanding and controlling water stability of MOF-74. *Journal of Materials Chemistry A, 4*(14), 5176–5183. https://doi.org/10.1039/C5TA10416E

[25] Degaga, G. D. (2018). *Physicochemical, spectroscopic properties, and diffusion mechanisms of small hydrocarbon molecules in MOF-74-Mg/Zn: A quantum chemical investigation*. Michigan Technological University.

[26] Howe, J. D., Morelock, C. R., Jiao, Y., Chapman, K. W., Walton, K. S., & Sholl, D. S. (2017). Understanding structure, metal distribution, and water adsorption in mixed-metal MOF-74. *The Journal of Physical Chemistry C, 121*(1), 627–635. https://doi.org/10.1021/acs.jpcc.6b11719

[27] Adhikari, D., Karki, R., Adhikari, K., & Pantha, N. (2024). First-principles study on the selective separation of toxic gases by Mg-MOF-74. *ACS Omega*. https://doi.org/10.1021/acsomega.3c08358

[28] Pham, T., Forrest, K. A., Banerjee, R., Orcajo, G., Eckert, J., & Space, B. (2015). Understanding the H2 sorption trends in the M-MOF-74 series (M= Mg, Ni, Co, Zn). *The Journal of Physical Chemistry C, 119*(2), 1078–1090. https://doi.org/10.1021/jp510253m

[29] Schoenecker, P. M., Carson, C. G., Jasuja, H., Flemming, C. J., & Walton, K. S. (2012). Effect of water adsorption on retention of structure and surface area of metal–organic frameworks. *Industrial & Engineering Chemistry Research, 51*(18), 6513–6519. https://doi.org/10.1021/ie202325p

[30] Li, Y., Wang, X., Xu, D., Chung, J. D., Kaviany, M., & Huang, B. (2015). H2O adsorption/desorption in MOF-74: Ab initio molecular dynamics and experiments. *The Journal of Physical Chemistry C, 119*(23), 13021–13031. https://doi.org/10.1021/acs.jpcc.5b02069

[31] Yang, D. A., Cho, H. Y., Kim, J., Yang, S. T., & Ahn, W. S. (2012). CO2 capture and conversion using Mg-MOF-74 prepared by a sonochemical method. *Energy & Environmental Science, 5*(4), 6465–6473. https://doi.org/10.1039/c1ee02234b

[32] Yun, J. H., He, Y., Otero, M., Düren, T., & Seaton, N. (2002). Adsorption equilibrium of polar/non-polar mixtures on MCM-41: Experiments and Monte Carlo simulation. In *Studies in Surface Science and Catalysis* (Vol. 144, pp. 685–692). Elsevier. https://doi.org/10.1016/S0167-2991(02)80197-5

[33] Slater, J. C. (1951). A simplification of the Hartree-Fock method. Physical Review, 81(3), 385. https://doi.org/10.1103/PhysRev.81.385

[34] Engel, E. (2011). Density functional theory. Springer. https://doi.org/10.1007/978-3-642-14090-7

[35] Hospital, A., Goñi, J. R., Orozco, M., & Gelpí, J. L. (2015). Molecular dynamics simulations: Advances and applications. Advances and Applications in Bioinformatics and Chemistry, 8, 37–47. https://doi.org/10.2147/AABC.S70333

[36] Mao, Q., Feng, M., Jiang, X. Z., Ren, Y., Luo, K. H., & van Duin, A. C. (2023). Classical and reactive molecular dynamics: Principles and applications in combustion and energy systems. Progress in Energy and Combustion Science, 97, 101084. https://doi.org/10.1016/j.pecs.2023.101084

[37] Frisch, M. (2009). Gaussian 09 (Revision D.01). Gaussian Inc.

[38] Plimpton, S., Crozier, P., & Thompson, A. (2007). LAMMPS-large-scale atomic/molecular massively parallel simulator. Sandia National Laboratories, 18, 43.

[39] Zhang, G., Liang, Y., Cui, G., et al. (2023). Grand canonical Monte Carlo simulation of the adsorption and separation of carbon dioxide and methane using functionalized Mg-MOF-74. Energy Reports, 9, 2852–2860. https://doi.org/10.1016/j.egyr.2023.01.121

[40] Berendsen, H. J., Grigera, J. R., & Straatsma, T. P. (1987). The missing term in effective pair potentials. Journal of Physical Chemistry, 91(24), 6269–6271. https://doi.org/10.1021/j100308a038

[41] Mercado, R., Vlaisavljevich, B., Lin, L. C., et al. (2016). Force field development from periodic density functional theory calculations for gas separation applications using metal–organic frameworks. The Journal of Physical Chemistry C, 120(23), 12590–12604. https://doi.org/10.1021/acs.jpcc.6b03393

[42] Du, Z., Nie, X., Deng, S., et al. (2020). Comparative analysis of calculation methods of adsorption isosteric heat: Case study of CO2 capture using MOFs. Microporous and Mesoporous Materials, 298, 110053. https://doi.org/10.1016/j.micromeso.2020.110053

[43] Chatterjee, S., Debenedetti, P. G., Stillinger, F. H., & Lynden-Bell, R. M. (2008). A computational investigation of thermodynamics, structure, dynamics and solvation behavior in modified water models. The Journal of Chemical Physics, 128(12). https://doi.org/10.1063/1.2841127

[44] Metropolis, N., Rosenbluth, A. W., Rosenbluth, M. N., Teller, A. H., & Teller, E. (1953). Equation of state calculations by fast computing machines. The Journal of Chemical Physics, 21(6), 1087–1092. https://doi.org/10.1063/1.1699114

[45] Babaei, S., Ghasemzadeh, H., & Tesson, S. (2023). Methane adsorption of nanocomposite shale in the presence of water: Insights from molecular simulations. Chemical Engineering Journal, 475, 146196. https://doi.org/10.1016/j.cej.2023.146196

[46] Peng, D. Y., & Robinson, D. B. (1976). A new two-constant equation of state. Industrial & Engineering Chemistry Fundamentals, 15(1), 59–64. https://doi.org/10.1021/i160057a011

[47] Nosé, S. (1984). A unified formulation of the constant temperature molecular dynamics methods. The Journal of Chemical Physics, 81(1), 511–519. https://doi.org/10.1063/1.447334

[48] Kirkwood, J. G., & Boggs, E. M. (1942). The radial distribution function in liquids. The Journal of Chemical Physics, 10(6), 394–402. https://doi.org/10.1063/1.1723737

[49] Listyarini, R. V., Gamper, J., & Hofer, T. S. (2023). Storage and diffusion of carbon dioxide in the metal-organic framework MOF-5: A semi-empirical molecular dynamics study. The Journal of Physical Chemistry B, 127(43), 9378–9389. https://doi.org/10.1021/acs.jpcb.3c04155

[50] Wang, Z., Zhang, Y., Chen, S., Fu, Y., Li, X., & Pei, J. (2021). Molecular simulation of adsorption and diffusion of CH4 and H2O in flexible metal-organic framework ZIF-8. Fuel, 286, 119342. https://doi.org/10.1016/j.fuel.2020.119342

[51] Lemmon, E. W. (2010). Thermophysical properties of fluid systems. NIST Chemistry WebBook. https://doi.org/10.18434/T4D303

[52] Shang, Z., Yang, Y., Zhang, L., et al. (2024). Hydrogen adsorption and diffusion behavior in kaolinite slit for underground hydrogen storage: A hybrid GCMC-MD simulation study. Chemical Engineering Journal, 487, 150517. https://doi.org/10.1016/j.cej.2024.150517

[53] Fatriansyah, J., Dhaneswara, D., Abdurrahman, M. H., Kuskendrianto, F. R., & Yusuf, M. (2019). Molecular dynamics simulation of hydrogen adsorption on silica. In IOP Conference Series: Materials Science and Engineering (Vol. 478, Article 012034). https://doi.org/10.1088/1757-899X/478/1/012034

[54] Liu, Y. (2006). Some considerations on the Langmuir isotherm equation. Colloids and Surfaces A: Physicochemical and Engineering Aspects, 274(1–3), 34–36.

[55] Lee, J. G. (2016). Computational materials science: An introduction. CRC Press. https://doi.org/10.1201/9781315368429

[56] Demontis, P., Stara, G., & Suffritti, G. B. (2003). Behavior of water in the hydrophobic zeolite silicalite at different temperatures: A molecular dynamics study. The Journal of Physical Chemistry B, 107(18), 4426–4436. https://doi.org/10.1021/jp0300849

[57] Fogarty, A. C., Coudert, F. X., Boutin, A., & Laage, D. (2014). Reorientational dynamics of water confined in zeolites. ChemPhysChem, 15(3), 521–529. https://doi.org/10.1002/cphc.201300928

[58] Salles, F., Kolokolov, D. I., Jobic, H., et al. (2009). Adsorption and diffusion of H2 in the MOF type systems MIL-47 (V) and MIL-53 (Cr): A combination of microcalorimetry and QENS experiments with molecular simulations. The Journal of Physical Chemistry C, 113(18), 7802–7812. https://doi.org/10.1021/jp811190g